X-615-64-279

NASA TM X-55135

THE EFFECT OF A VARIABLE ELECTRON TEMPERATURE ON THE EQUATORIAL ELECTRON DENSITY DISTRIBUTION IN THE UPPER IONOSPHERE

BY
RICHARD A. GOLDBERG

OCTOBER 1964

GODDARD SPACE FLIGHT CENTER
GREENBELT, MARYLAND
Ionosphere Preprint Series

THE EFFECT OF A VARIABLE ELECTRON TEMPERATURE ON THE EQUATORIAL ELECTRON DENSITY DISTRIBUTION IN THE UPPER IONOSPHERE

by

Richard A. Goldberg
NASA-Goddard Space Flight Center
Greenbelt, Maryland

ABSTRACT

By incorporating a model for the measured electron temperature distribution at the magnetic equator in the isothermal and temperature equilibrium theory of Goldberg, Kendall and Schmerling [J. Geophys. Res., 69, 417-427, 1964], it has been possible to gain further insight into the behavior of the equatorial geomagnetic anomaly under steady state and equinoctial conditions. In particular, it is shown that the measured deviation from thermal equilibrium in the bottomside ionosphere is very influential in allowing extension of the previous theoretical description of the geomagnetic anomaly well into the bottomside ionosphere and to higher latitudes than originally applicable. For completeness, the effect of gravitational variation is now included, but it is shown that this alone contributes only minor improvements to the original results. Finally, several less common properties in the behavior of the geomagnetic anomaly are investigated, and it is shown under what conditions these secondary effects will occur.

INTRODUCTION

The theory describing the equatorial electron density distribution under conditions of thermal equilibrium, equinox, and steady state, originally presented in Goldberg and Schmerling [1963, 1964] and improved upon in Goldberg, Kendall and Schmerling [1964] (to be referred to as GKS), has provided reasonably good agreement when comparison is made to the measured results of the Alouette Topside Sounder Satellite. Furthermore, Chandra and Goldberg [1964] (to be referred to as CG) have demonstrated that the rather artificial concept of field line diffusive equilibrium need not be employed to obtain the necessary equations, but instead, the neglect of collisions between charged and neutral particles is sufficient in this aim. This has enabled us to understand why the theoretical results agree best with data in the topside ionosphere, since this is the region where such an assumption is most reasonable.

Recent theoretical considerations (Hanson and Johnson, 1961; Hanson, 1962; Dalgarno et al, 1963) and recent measurements with rocket probes (Spencer et al, 1962; Brace et al, 1963) and radar backscatter techniques (Evans, 1962 and 1964; Bowles, 1964) have now demonstrated that thermal equilibrium (electron temperature T_e = ion temperature T_i) does not occur in the lower F region ionosphere during the day including that time when the electron density is experiencing nearly steady conditions. It is the purpose of this paper to provide a simple analytical approach for including a temperature model, based on the theoretical or measured T_e distribution, in the theory discussed in GKS and CG, and to demonstrate the possible effects of deviation from conditions of thermal equilibrium on the topside electron density distribution. Furthermore, it will be shown how inclusion of this T_e distribution has allowed extension of the theory into part of the bottomside F layer. Comparison with data is also made to provide a possible explanation of several features of the geomagnetic anomaly heretofore unexplained. For completeness, the effects of variable gravity are also included and the slight

modifications in the results due to this effect are demonstrated.

SYMBOLS

$\vec{B}$	magnetic field of earth
e	absolute value of electron charge
$\vec{g}$	gravity
H_e	electron density scale height
H_i	ionizable constituent scale height; cf. (16)
H_p	value of H_i at r_p
H_T	scale factor of temperature
H_τ	cf. (7)
$\vec{h}$	unit vector in direction of $\vec{B}$
h_mF2	height of F2 layer electron density peak
I	magnetic dip angle; cf. (10)
$\vec{i}_r, \vec{i}_\theta$	polar coordinate unit vectors
$\vec{J}$	current density; cf. (3)
K	value of T_e/T_i at r_p
k	Boltzmann's constant
m	mass
N,n	number density; cf. (2)
N_{mo}	equatorial peak electron density
N_mF2	F2 layer peak electron density
p	pressure
R	mean radius of earth (6370 km)

r	radial height ($r = z + R$)
r_{mo}	height of equatorial peak electron density
r_o	equatorial radial height
r_p	radial height of temperature peak
T	temperature
$\vec{v}$	velocity
z	altitude
θ	colatitude
ν_{jk}	collision frequency between j^{th} and k^{th} particles
τ	average of electron and ion temperatures; cf. (6)

SUBSCRIPTS

e,i,n	electrons, ions, and neutral particles respectively
m	peak value
mo	equatorial peak value

THE FUNDAMENTAL EQUATION

From CG, combination of the equations of motion for electrons and ions provides

$$Nm_e \nu_{en} \vec{v}_e + \frac{Nm_i m_n}{m_i + m_n} \nu_{in} \vec{v}_i =$$

$$-\nabla p_e - \nabla p_i + N m_i \vec{g} + \vec{J}X\vec{B} \qquad (1)$$

where we have assumed

$$v_n << v_e,\ v_i$$

$$m_e << m_i,\ m_n$$

$$n_e = n_i = N \qquad (2)$$

In (1) and (2), the subscripts e, i, and n refer to electrons, ions, and neutrals respectively; p is pressure; n is number density; ν_{jk} is collision frequency between the j^{th} and k^{th} particles; m is mass; v is velocity; g is gravitational acceleration; B is the earth's magnetic field; and J is current density defined as

$$\vec{J} = Ne\ (\vec{v}_i - \vec{v}_e) \qquad (3)$$

where e is the absolute value of electron charge.

If now, we assume that ν_{en} and ν_{in} are sufficiently small to allow neglect of the drag forces, then

$$-\nabla p_e - \nabla p_i + N\, m_i \vec{g} + \vec{J}\times\vec{B} = 0 \qquad (4)$$

Assuming the electrons and ions behave as ideal gases and taking the field line component of (4), we obtain

$$[-\,Nk\,\nabla(T_e+T_i) - (T_e+T_i)k\,\nabla N + N\, m_i \vec{g}]\cdot\vec{h} = 0 \qquad (5)$$

where T_j is the temperature of the j^{th} type particle, k is Boltzmann's constant, and $\vec{h}$ is a unit vector in the direction of the earth's magnetic field.

Let us define

$$\tau = \frac{T_e+T_i}{2} \tag{6}$$

$$H_\tau = \frac{k\,\tau}{m_i g} \tag{7}$$

Then

$$\left(\frac{\nabla\tau}{\tau} + \frac{\nabla N}{N} + \frac{\vec{i}_r}{2H_\tau}\right)\cdot\vec{h} = 0 \tag{8}$$

where $\vec{i}_r$ is a unit vector in the radial direction. If we assume that the earth's magnetic field is a dipole lying in the r, θ plane, we obtain

$$\frac{1}{\tau}\left(\frac{\partial\tau}{\partial r}\sin I + \frac{1}{r}\frac{\partial\tau}{\partial\theta}\cos I\right) + \frac{1}{N}\left(\frac{\partial N}{\partial r}\sin I + \frac{1}{r}\frac{\partial N}{\partial\theta}\cos I\right) + \frac{\sin I}{2H_\tau} = 0 \tag{9}$$

where I is the magnetic dip angle defined by

$$\tan I = 2\cot\theta \tag{10}$$

and θ is geomagnetic colatitude. (In the following discussion, all coordinates given are geomagnetic.) As pointed out in CG, (9) can be written in total dervative form as

$$\frac{d\tau}{\tau} + \frac{dN}{N} + \frac{dr}{2H_\tau} = 0 \tag{11}$$

provided the integration is carried out along a field line. The solution of (11) is

$$N(r,\theta) = N(r_o) \frac{\tau(r_o)}{\tau(r,\theta)} e^{-\int_{r_o}^{r} \frac{dr}{2H\tau}} \qquad (12)$$

where r_o is the equatorial height of the field line of integration, i.e.

$$r_o = r \csc^2\theta \qquad (13)$$

and $N(r_o)$, $\tau(r_o)$ represent the vertical distributions of N and τ at the equator.

THE BOUNDARY CONDITIONS

From (12), it is clear that the complete temperature distribution, given by $\tau(r,\theta)$, must be known in addition to the radial distribution of N at the equator, $N(r_o)$, before $N(r,\theta)$ can be determined uniquely. In previous work, $\tau(r,\theta)$ has simply been specified as a constant everywhere. We now investigate the properties of the theoretical electron density distribution when we include a simple radial model for τ based on measurement and theory.

Recent rocket probe measurements (Spencer, et al, 1962 and Brace, et al, 1963) at Wallops Island, Virginia, show a vertical electron temperature profile under quiet day conditions which departs from the ion temperature at 150 km, peaks between 200 and 250 km with a value of $T_e \approx 2\ T_i$, and then returns to the $T_i = T_e$ value at about 350 km. Evans [1962] obtains a similar type behavior and later [1964] shows improved results which indicate a peak at 300 km and a return to $T_e/T_i = 1$ above 700 km for radar backscatter measurements in the midlatitude region of Boston, Mass. The only measurements available in the equatorial region are those of Bowles [1964] using the backscatter technique and he reports a T_e/T_i peak value of 2 occurring at about 275 km. Furthermore, he never finds $T_e/T_i > 1$ above 400 km.

Hanson and Johnson [1961], Hanson [1962] and Dalgarno el al [1963] have presented theoretical models for T_e/T_i based on local EUV heating which result in similar type profiles to those measured, viz. $T_e/T_i = 2$ at the peak with the peak occurring between 200 and 250 km. The theoretical models are probably most representative of the equatorial regions where EUV heating is most likely to predominate. The theoretical peak height is somewhat lower than that reported by Bowles [1964] but Dalgarno et al [1963] explain that their lower value for the peak can be attributed to an underestimate of the cooling rate by neglect of the contribution from vibrational excitations. They also state that one should expect a more rapid cooling rate in a warmer atmosphere and this appears to indicate a higher altitude for the T_e/T_i peak at times of higher sunspot number. These are important considerations in selecting the numerical values for the height of the electron temperature peak (r_p) in the next section.

The results discussed above clearly demonstrate the absence of thermal equilibrium in the lower F region of the ionosphere. Unfortunately, the data and theoretical models available are rather limited and the exact behavior and distributional shape is currently rather uncertain. As a reasonable first guess, we therefore choose a simple analytic distribution for T_e which is representative of any of the above profiles but which does not fit any of them in an exact sense. We also consider the temperature behavior to be independent of latitude in the equatorial region under consideration (i.e. from 20° N to 20° S).

An expression which possesses these qualifications is

$$T_e = T_i \left[1 + \frac{K-1}{1 + \dfrac{(r-r_p)^2}{H_T^2}} \right] \qquad (14)$$

where K is the ratio T_e/T_i at the peak height (r_p) of the T_e distribution and H_T is a scaling factor which governs the thickness of the T_e distribution and which will be referred to as the thermal scale height. A typical plot of (14) is shown in Figure 1 for various values of H_T and for r_p = 6650 km. From (14), we obtain

$$\tau(r,\theta) = \tau(r) = \frac{T_i}{2}\left[2 + \frac{K-1}{1+\dfrac{(r-r_p)^2}{H_T^2}}\right] \qquad (15)$$

Although the effect of the gravitational height dependence is small, we include it for completeness in the work which follows. The scale height of the ionizable constituent is given by

$$H_i = \frac{kT_i}{m_i g} \qquad (16)$$

If we define H_p as that value of H_i at the height r_p, i.e. the matching point, and we treat T_i as constant in the region under consideration, then

$$H_i = \frac{r^2}{r_p^2} H_p \qquad (17)$$

With these definitions, we have

$$H_\tau = \frac{H_p}{2}\frac{r^2}{r_p^2}\left[2 + \frac{K-1}{1+\dfrac{(r-r_p)^2}{H_T^2}}\right] \qquad (18)$$

The form of H_τ given by (18) allows explicit integration of the integral in (12). We obtain

$$-\int_{r_o}^{r} \frac{dr}{2H_T} = \frac{r_p^2 \left[F_1 + F_2 + F_3 + F_4\right]}{2H_p\left[r_p^2 + \frac{H_T^2(K+1)}{2}\right]^2} \qquad (19a)$$

where

$$F_1 = \left[r_p^2 - H_T^2 \frac{(K+1)}{2}\right]\left[\frac{H_T(K-1)}{2\left(\frac{K+1}{2}\right)^{\frac{1}{2}}}\right]\left[\tan^{-1}\left(\frac{r-r_p}{H_T\left[\frac{K+1}{2}\right]^{\frac{1}{2}}}\right) - \tan^{-1}\left(\frac{r_o-r_p}{H_T\left[\frac{K+1}{2}\right]^{\frac{1}{2}}}\right)\right] \qquad (19b)$$

$$F_2 = r_p H_T^2 \left(\frac{K-1}{2}\right) \ln\left[\frac{(r_o-r_p)^2 + H_T^2\left(\frac{K+1}{2}\right)}{(r-r_p)^2 + H_T^2\left(\frac{K+1}{2}\right)}\right] \qquad (19c)$$

$$F_3 = 2r_p\left[\frac{K-1}{2} H_T^2 \ln r/r_o\right] \qquad (19d)$$

and

$$F_4 = \frac{r_o-r}{r\, r_o}\left[\left(r_p^2 + \frac{H_T^2(K+1)}{2}\right)\left(H_T^2 + r_p^2\right)\right] \qquad (19e)$$

Finally, we must apply an analytic form for $N(r_o)$. Although Chandra (1962) formulated an improved functional form for N(r) than that described by the simple Chapman function and this has been incorporated in the results of CG, it is necessary to return to the simple Chapman function in the work that follows in order to make direct comparison with Goldberg, Kendall and Schmerling (1964). Hence, we let

$$N(r_o) = N(r_{mo}) e^{\frac{1}{2}\left[1 - \frac{r_o-r_{mo}}{H_e} - e^{-\frac{r_o-r_{mo}}{H_e}}\right]} \qquad (20)$$

where H_e is the electron density scale height at the equator and N_{mo} is the value of electron density at the vertical peak height r_{mo}.

NUMERICAL ANALYSIS AND DISCUSSION

A. The Effect of Gravity

The expressions given by (15), (19) and (20) have been incorporated in (12) to provide an analytic expression for the electron density near the geomagnetic equator above and below the electron density peak under conditions of steady state and equinox. This expression has then been programmed on an IBM 7094 to allow extensive study of its behavior under wide variations in the temperature parameters. The discussion which follows demonstrates how adjustment of the parameters governing the temperature distribution leads to variations in the properties of the geomagnetic anomaly.

Before investigating the actual effect of a variable T_e, let us first study the change induced by simply adding the gravity variation. This is obtained by replacing H_τ with H_i and treating $\tau(r,\theta)$ as a constant in (12). Then

$$N(r,\theta) = N(r_o)e^{\frac{r\cos^2\theta}{2H_i}} \qquad (21)$$

where H_i possesses the functional dependence on height given by (17). This can be compared to the constant H_i result employed in GKS, viz.

$$N(r,\theta) = N(r_o)e^{\frac{r\cot^2\theta}{2H_p}} \qquad (22)$$

where H_2 of GKS is now H_p. (In the discussion and results which follow, the scale height of the electron density distribution H_e has also replaced 1/k in GKS notation).

Comparison of (21) and (22) shows that very little change in results should be expected in that region of latitude where $\cot\theta$

and cosθ are comparable in magnitude. This encompasses nearly the entire region of our interest. This conclusion is borne out by numerical comparison of (21) and (22) for cases in which $H_p/H_e > 1$. A more important result is obtained for cases presented in GKS for $H_p/H_e \leq 1$. In that paper it was shown that angular peaks could not be obtained for this range of selection in parameters, although the initial rise with latitude behaved in equivalent manner to the geomagnetic anomaly. The simple inclusion of gravity now rectifies this situation by allowing angular peaks to form for these cases.

A comparison of the 380 km and 480 km electron density profiles with and without gravity variation for $H_p/H_e = 1$ is shown in Figure 2 using the numerical parameters given in Table 1 (The altitude z is related to radial distance r by r = z + 6370 km). Curve a represents the constant g case given by (22). Curves b and c represent variable g(r) cases in which the matching of H_i with H_p is taken to be at two different heights, viz. 6650 and 6850 km, respectively. We first note that the effect of varying the matching point is rather small and has little if any influence on the features we wish to discuss. We also find that regardless of matching point height, the curves stay relatively close even at high latitudes. The generation of an angular peak for $r_p = 6650$ km is not surprising since $H_i/H_p > 1$ everywhere above r_p. However, it is surprising to find this result for the 380 km (6750 km) profile when $r_p = 6850$, since $H_i/H_e < 1$ at this height. This result occurs for all cases investigated and we must conclude that although gravity is a small effect in altering the slope of the curves, as comparison of curves 2b and 2c demonstrate, it is a strong effect in providing a more realistic description of the geomagnetic anomaly should it occur under conditions where $H_p/H_e \leq 1$.

B. The Effect of Temperature

Although inclusion of height dependent gravity, g(r), appears to resolve the problem of theoretically describing the geomagnetic

anomaly when $H_i/H_e \leq 1$, it has been shown in CG that this condition is a rather unlikely situation to occur on both empirical and physical grounds. We therefore restrict ourselves in the discussion which follows to $H_i/H_e > 1$.

There are seven parameters to be varied in this problem on the basis of empirical conditions, viz. N_{mo}, r_{mo}, H_e, H_p, H_T, r_p and K. In GKS, it was shown that variation of the first four parameters leads to a description of the equinoctial noontime geomagnetic anomaly during various phases of the solar cycle. Furthermore, although differences in the magnitude and height range of the anomaly occur between high and low sunspot number, no changes in the basic features ascribed to this effect are expected. We will, therefore, limit ourselves to an analysis of the high sunspot case with the knowledge that the results obtained are similar but less pronounced for the intermediate and low sunspot cases. The choice of values for the first four parameters listed above have been made to coincide with GKS by selecting

$$N_{mo} = 19.25 \times 10^5 \text{ electrons/cm}^3,$$

$$H_e = 100 \text{ km}, \quad r_{mo} = 6850 \text{ km},$$

and

$$H_p = 112.5 \text{ km}.$$

Selection of H_p at the given value insures $H_i/H_e > 1$ in the entire region of interest. The values of the other numerical parameters used are given in Table 1. (These values are selected to coincide as accurately as possible with the temperature profile discussed earlier).

We can therefore reduce the problem to a three parameter study; H_T and K which determine the thickness and magnitude of the T_e peak respectively; and r_p, which determines the relative distance between

the electron temperature and density maxima.

Figure 3 represents a sequence of electron density constant height profiles under the effects of T_e variation. Figure 4 represents an equivalent set of vertical profiles. The temperature profile used is illustrated in Figure 1 with parametric values selected for reasons discussed in a previous section.

Comparison of Figure 3 to the thermal equilibrium, constant gravity results given in GKS shows very little modification of the curves out to the angular peak. On the high latitude side of the peak, however, we find a more rapid decrease of electron density in better agreement with measured profiles. This effect is due primarily to the inclusion of the gravitational variation and not the variation in T_e.

A more important result, and one which is entirely due to a variable T_e, is evident in Figure 4. We now find qualitative results which match measured data to a height nearly two electron scale heights (H_e) below the equatorial F2 peak before discrepancies begin to occur. Since the vertical profiles show a departure from measurement below this height, it appears that the neglect of friction terms in the equations of motion is no longer valid below this region. Nevertheless, it is a valuable extension of the theory to find that the effect of collisions can be neglected to heights well below the equatorial F2 peak, especially since it appeared by the results of GKS that collisions were important everywhere below this peak, i.e. in GKS results obtained below the peak do not agree with data and the vertical peaks shown in Figure 4 of this work could not be produced.

The variation of the peak electron density N_mF2 with latitude is given in Figure 5. We observe that a variable T_e produces angular peaks in N_mF2 in accord with measurement, (cf. Croom et al, 1959) whereas in GKS, it was shown that thermal equilibrium is incapable of producing the angular "turnover". Furthermore, this result must be attributed to a variable T_e, since inclusion of

variable gravity alone does not alter the results for this parameter given in GKS. The variation of the height of the F2 peak, h_mF2, is also given in Figure 5. We observe a leveling out of this height at higher latitudes in accord with measurement (cf. Thomas, 1962), a result which also is not available under thermal equilibrium considerations. A study of these quantities show that their magnitude and shape are very stable to wide variations in K, H_T and $r_{mo}-r_p$, except when K and H_T become very small, i.e. $H_T \leq 20$, $K \leq 1.2$. At these and smaller values we find a rapid transition into the forms published in GKS for thermal equilibrium, in which h_mF2 drops steadily with latitude and N_mF2 rises with latitude without showing any angular peaks.

Figure 6A demonstrates the variation of a typical constant height profile with r_{mo}, viz. 380 km, holding K and H_T fixed. We note that as r_p approaches r_{mo}, the original angular peak converts into a sharper peak adjacent to a relatively flat "ledge". Further study has shown that this effect is not dependent on the absolute value of r_{mo} or the relative distance between the actual constant height profile and r_{mo}. Instead, this behavior is exclusively dependent on $r_{mo}-r_p$.

Because the results which follow depend only on the relative separation $r_{mo}-r_p$ and not on the absolute values of r_p and r_{mo}, and because of the discussion in an earlier section explaining how r_p can actually be larger in a warmer (high sunspot number) ionosphere, we have selected the relatively high value of $r_p \approx r_{mo} = 6850$ km. If the condition $r_p = r_{mo}$ occurs at a lower height, the same results will occur simply shifted this distance in altitude. From Figure 6A we find that the new effect is not present until r_p is very nearly equal to r_{mo}, and becomes more pronounced as r_p increases (or r_{mo} decreases).

Although the above effect is not always present, it has appeared in measurements of King et al (1963), an example of which is shown in Figure 7. No attempt has been made to accurately fit this par-

ticular profile, however, since there are many combinations of the seven parameters available for such a fit and the profiles showing this property best in the published literature do not always represent noon equinox conditions. Nevertheless, the effect does occur, and this indicates that the electron temperature and density peaks do lie relatively close together at certain times. During such an occurrence, we would expect the geomagnetic anomaly to appear in a form similar to the result given in Figure 8, where we notice a low latitude "ledge" replacing the low latitude "trough" at higher altitudes. We also note a reduction in the height above which the anomaly disappears.

The sequence of vertical profiles corresponding to Figure 8 ($r_p = r_{mo}$) are shown in Figure 9. We find that this extreme lowering of the electron density peak (or raising of the temperature peak) leads to an additional small "bump" in the topside region.

Other smaller effects are also seen upon more detailed study of the results. For example, if $r_{mo}-r_p$ is of the order .75 H_e (see Figure 6A), we find the sequence of horizontal profiles illustrated in Figure 10, demonstrating a much smaller ledge occurring on the low latitude side of the angular peaks with no ledge present on the high latitude side. The topside results in this case are identical to those of Figure 3. The determination of this behavior from measurement is difficult, however, because of the small magnitude of the effect.

As partially shown in Figures 6B and 6C, a study of the variations of both K (temperature peak magnitude) and H_T (temperature peak thickness) do not lead to any new conclusions but form a consistent picture, i.e. as K decreases, the ledge gradually disappears leaving the normal horizontal profile for the variable gravity case. As H_T decreases, the effect first sharpens before disappearing for $H_T \leq 15$ km. Similarly, as K and H_T decrease, the topside "bump" in the vertical profile (cf. Figure 9) gradually lowers and blends with the

single peak obtained under variable gravity conditions alone. Increasing H_T and K improves the results on the bottomside by reducing the magnitude of the electron density profiles to more reasonable values in this region. Increasing H_T also sharpens the angular peak slightly. Finally, if we consider cases of very large H_T, such as H_T = 1000 km, we find a behavior very similar to the H_T = 0 situation. This demonstrates that it is the gradient of T_e/T_i, and not its magnitude, which is mostly responsible for the results involving the effect illustrated in Figure 7.

SUMMARY AND CONCLUSIONS

The theory presented in GKS has been extended to include the effects of the variation in gravity andan electron temperature profile based upon empirical and theoretical results. This extension in the theory has led to distinct improvements in the theoretical description of the geomagnetic anomaly when comparison with data is made.

The inclusion of gravitational variation alone has led to an increased gradient on the high latitude side of the theoretical constant height profiles representing the geomagnetic anomaly, this being in better accord with measurement. Furthermore, for the cases in which $H_i/H_e \leq 1$, we now find angular peaks occurring in the constant height profiles, something which was not available under constant gravity considerations.

The inclusion of an electron temperature vertical profile creates results which are far more remarkable, however. We now obtain a description of the geomagnetic anomaly to heights as low as $2H_e$ below the F2 peak at the equator, thereby indicating that the neglect of friction or collision terms in the equation of motion is allowable down to these heights. The theoretical behavior of N_mF2 and h_mF2 are also found to agree with measurement out to midlatitudes and an angular peaking of N_mF2 is seen to occur. These are results which

could not be obtained in GKS under isothermal conditions and thermal equilibrium.

Although T_i has been treated as a constant in the derivation of the expression used to obtain these results, this is not considered to be a serious limitation in the theory since the major gradients in T_i currently appear to be considerably smaller than those in T_e and occur in the very lowest sector of the region under consideration.

Further study with a variable T_e shows that as the height of the electron temperature and density peaks approach one another, we can expect to find an interesting change in the shape of the horizontal electron profiles describing the geomagnetic anomaly. Experimental evidence is presented to show that this behavior does occur at certain times. We also find that the slope of the electron temperature peak rather than its magnitude is more responsible for this effect. In addition, the vertical profiles undergo a slight modification with the appearance of a small "bump" in the topside above h_mF2 during its occurrence. It should be noted, however, that the evidence given in Figure 7 is a topside result and the theoretical results of Figure 8 do not show this effect extending into the topside. Assuming that 431 km was slightly above r_{mo} in Figure 7, we must conclude that either r_p was slightly higher than r_{mo} or that $r_p = r_{mo}$ with the temperature peak exhibiting a sharp gradient (large K, small H_T) on that day, since these are the only possible methods for theoretically obtaining this effect in the topside with the temperature profile assumed. (Naturally, a different electron temperature profile, such as one which possesses a secondary peak in the topside, should not be ruled out as a possible cause of observing this effect in the topside). Since r_{mo} decreases rapidly with sunspot number, we would expect the above behavior to be most frequent during the low sunspot number period of the solar cycle.

Finally, several secondary features originating from the theory due to the magnitude of the separation between N and T_e peaks ($r_{mo}-r_p$) are discussed, but this type of "fine structure" is considered too small to be seen at this time.

Acknowledgements

I am grateful for the valuable assistance given to me in the programming and numerical analysis of this work by Christopher E. Bock and William M. Litman. I also offer my deepest thanks to Dr. S. J. Bauer for critically reading the manuscript and making several helpful suggestions.

REFERENCES

Bowles, K. L., Private Communication, 1964.

Brace, L. H., N. W. Spencer and G. R. Carignan, Ionosphere Electron Temperature Measurements and their Implications, J. Geophys. Res. 68, 5397-5412, 1963.

Chandra, S., Electron Density Distribution in the Upper F Region, J. Geophys. Res., 68, 1937-1942, 1963.

Chandra, S. and R. A. Goldberg, Geomagnetic Control of Diffusion in the Upper Atmosphere, J. Geophys. Res. 69, 3187-3197, 1964.

Croom, S., A. Robbins, and J. O. Thomas, Two Anomalies in the Behavior of the F2 Layer of the Ionosphere, Nature 184, 2003, 1959.

Dalgarno, A., M. F. McElroy and R. J. Moffett, Electron Temperatures in the Ionosphere, Planet. Space Sci., 11, 463-484, 1963.

Evans, J. V., Diurnal Variation of the Temperature of the F Region, J. Geophys. Res., 67, 4914-4920, 1962.

Evans, J. V., Ionospheric Temperatures during the Launch of NASA Rocket 8.14 on July 2, 1963, J. Geophys. Res., 69, 1436-1444, 1964.

Goldberg, R. A. and E. R. Schmerling, The Distribution of Electrons Near the Magnetic Equator, J. Geophys. Res., 67, 3813-3815, 1962.

Goldberg, R. A. and E. R. Schmerling, The Effect of Diffusion on the Equilibrium Electron Density Distribution in the F Region near the Geomagnetic Equator, J. Geophys. Res., 68, 1927-1936, 1963.

Goldberg, R. A., P. C. Kendall and E. R. Schmerling, Geomagnetic Control of the Electron Density in the F Region of the Ionosphere, J. Geophys. Res. 69, 417-427, 1964.

Hanson, W. B., Electron Temperatures in the Upper Atmosphere, Space Research, Proc. Intern. Space Sci. Symp., 3rd, Washington, 1962, edited by W. Priester pp. 282-302, North-Holland Publishing Company, Amsterdam, 1962.

Hanson, W. B. and F. S. Johnson, Electron Temperatures in the Ionosphere, paper presented at Tenth International Astrophysical Colloquium, Liege, Belgium, 1961.

King, J. W., D. Eccles, P. A. Smith, P. Dannahy, A. Legg, E. O. Olatunji, K. Rice, G. Webb and M. Williams, Further Studies of the Topside Ionosphere Based on the Topside Sounder Satellite Data, DSIR Radio Research Station Report No. RRS/I.M. 112 December 1963.

Spencer, N. W., L. H. Brace and G. R. Carignan, Electron Temperature Evidence for Nonthermal Equilibrium in the Ionosphere, J. Geophys. Res. 67, 157-175, 1962.

Thomas, J. O., "The Electron Density Distribution in the F Region of the Ionosphere", in Electron Density Profiles edited by B. Maehlum, Pergamon Press, 1962.

LIST OF FIGURES

TABLE

TABLE 1.

Figure	Curve	r_p (km)	H_T (km)	K
1	-	6650	Variable	2
2	a	-	0	1
	b	6650	0	1
	c	6850	0	1
3	-	6650	40	2
4	-	6650	40	2
5	-	6650	40	2
6A	-	Variable	40	2
6B	-	6850	40	Variable
6C	-	6850	Variable	2
8	-	6850	40	2
9	-	6850	40	2
10	-	6775	40	2

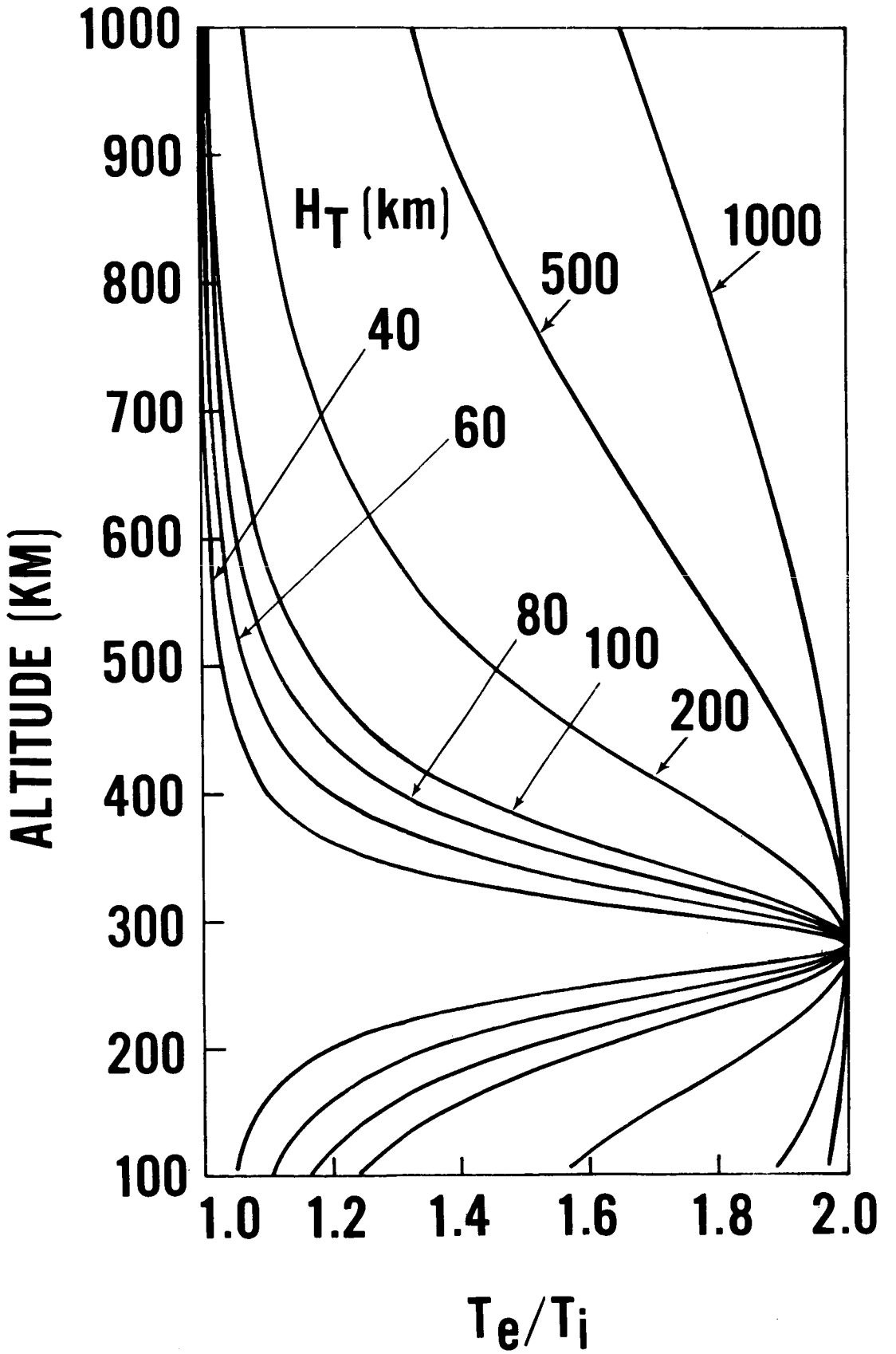
1000
900
800
700
600
500
400
300
200
100
ALTITUDE (KM)
H_T (km)
1000
500
40
60
80
100
200
1.0
1.2
1.4
1.6
1.8
2.0
T_e/T_i

Figure 1.

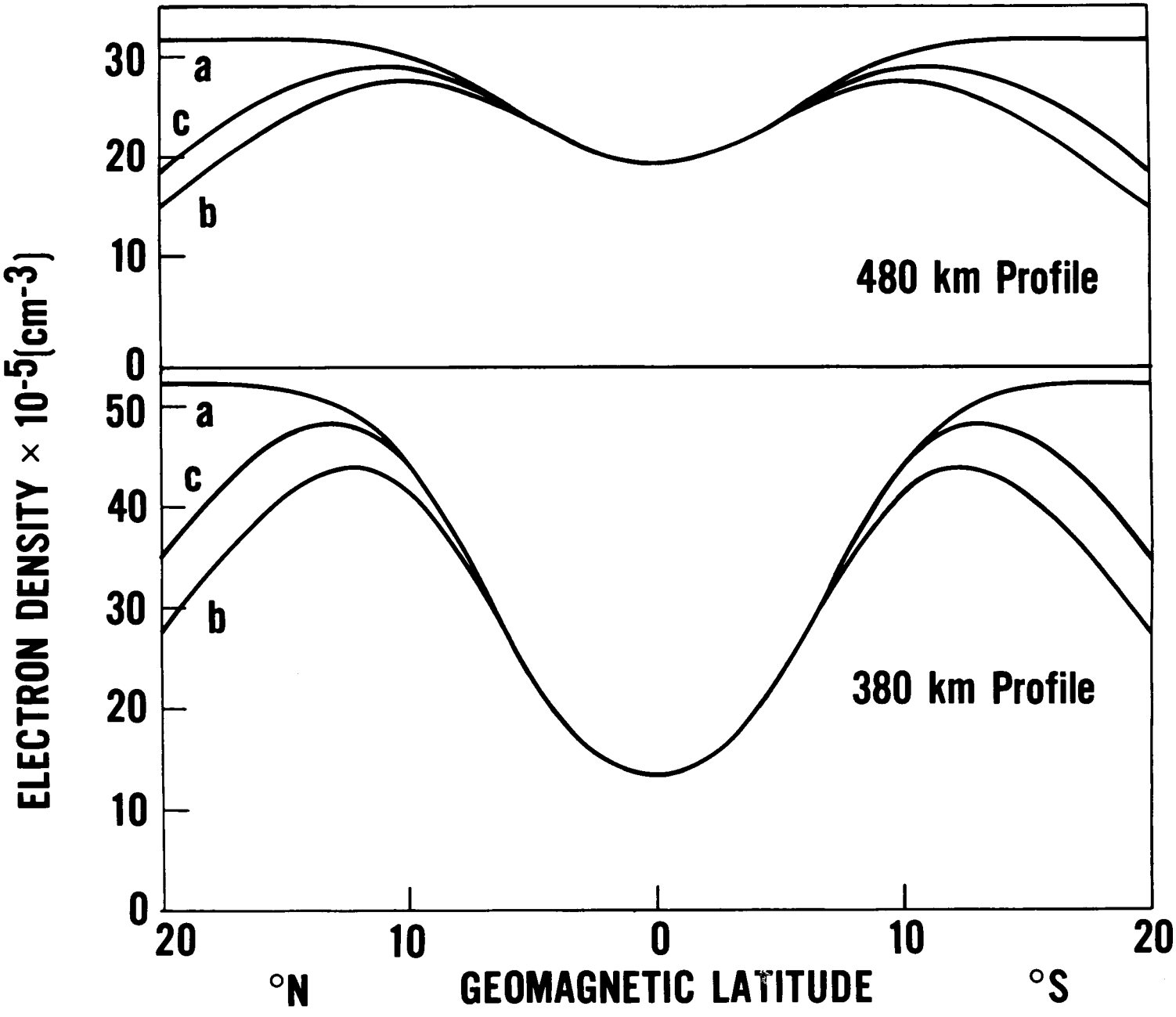
ELECTRON DENSITY × 10-5(cm-3)
30
20
10
0
a
c
b
480 km Profile
50
40
30
20
10
0
a
c
b
380 km Profile
20
10
0
10
20
°N
GEOMAGNETIC LATITUDE
°S

Figure 2.

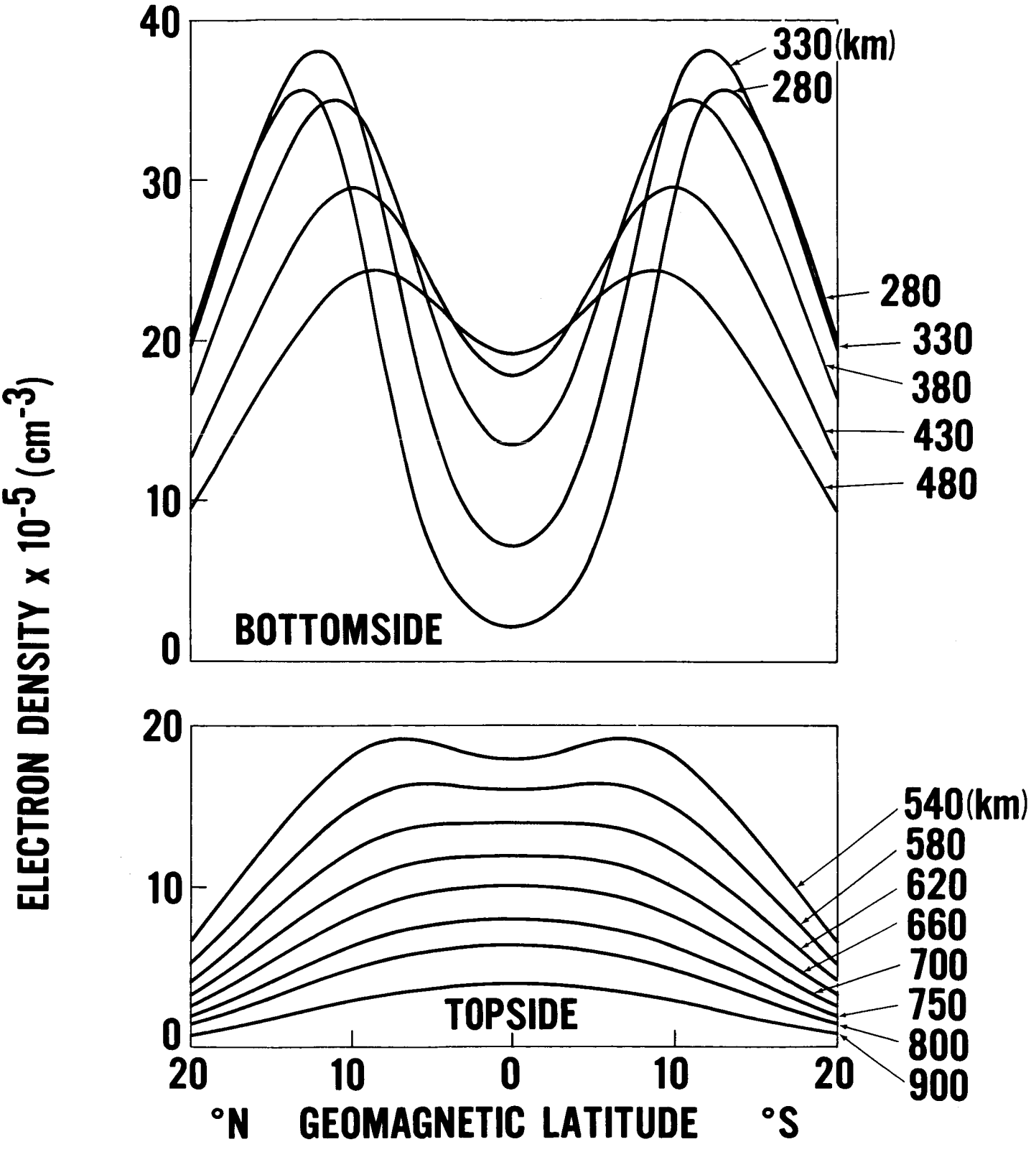
ELECTRON DENSITY x 10^{-5} (cm^{-3})
40
30
20
10
0
330(km)
280
280
330
380
430
480
BOTTOMSIDE
20
10
0
540(km)
580
620
660
700
750
800
900
TOPSIDE
20
10
0
10
20
°N GEOMAGNETIC LATITUDE °S

Figure 3.

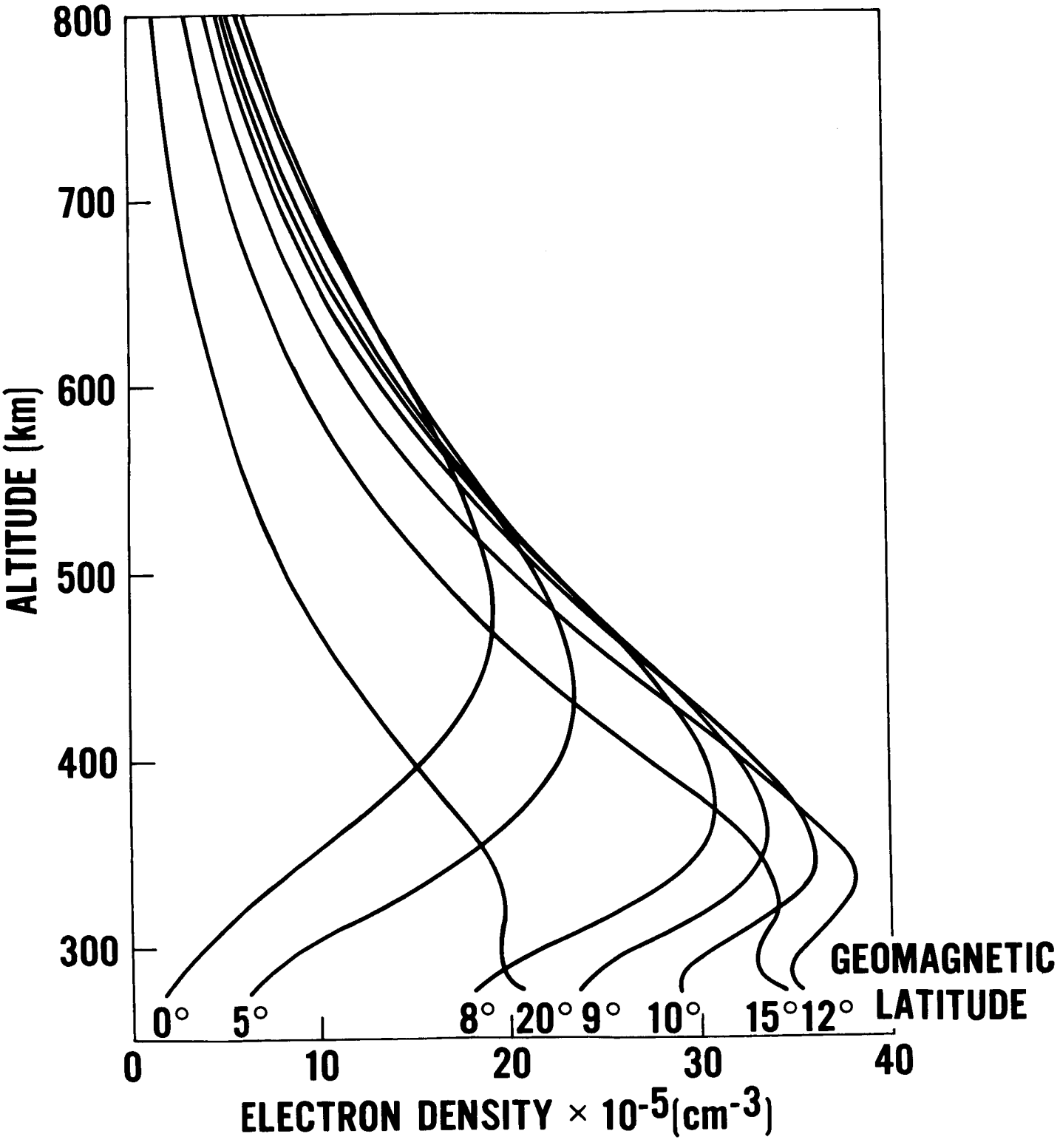
800
700
600
500
400
300
ALTITUDE (km)
0°
5°
8°
20°
9°
10°
15°
12°
GEOMAGNETIC LATITUDE
0
10
20
30
40
ELECTRON DENSITY × 10-5(cm-3)

Figure 4.

500
400
300
hm F2 (km)
40
30
20
Nm F2 × 10−5 (cm-3)
20
10
0
10
20
°N
GEOMAGNETIC LATITUDE
°S

Figure 5.

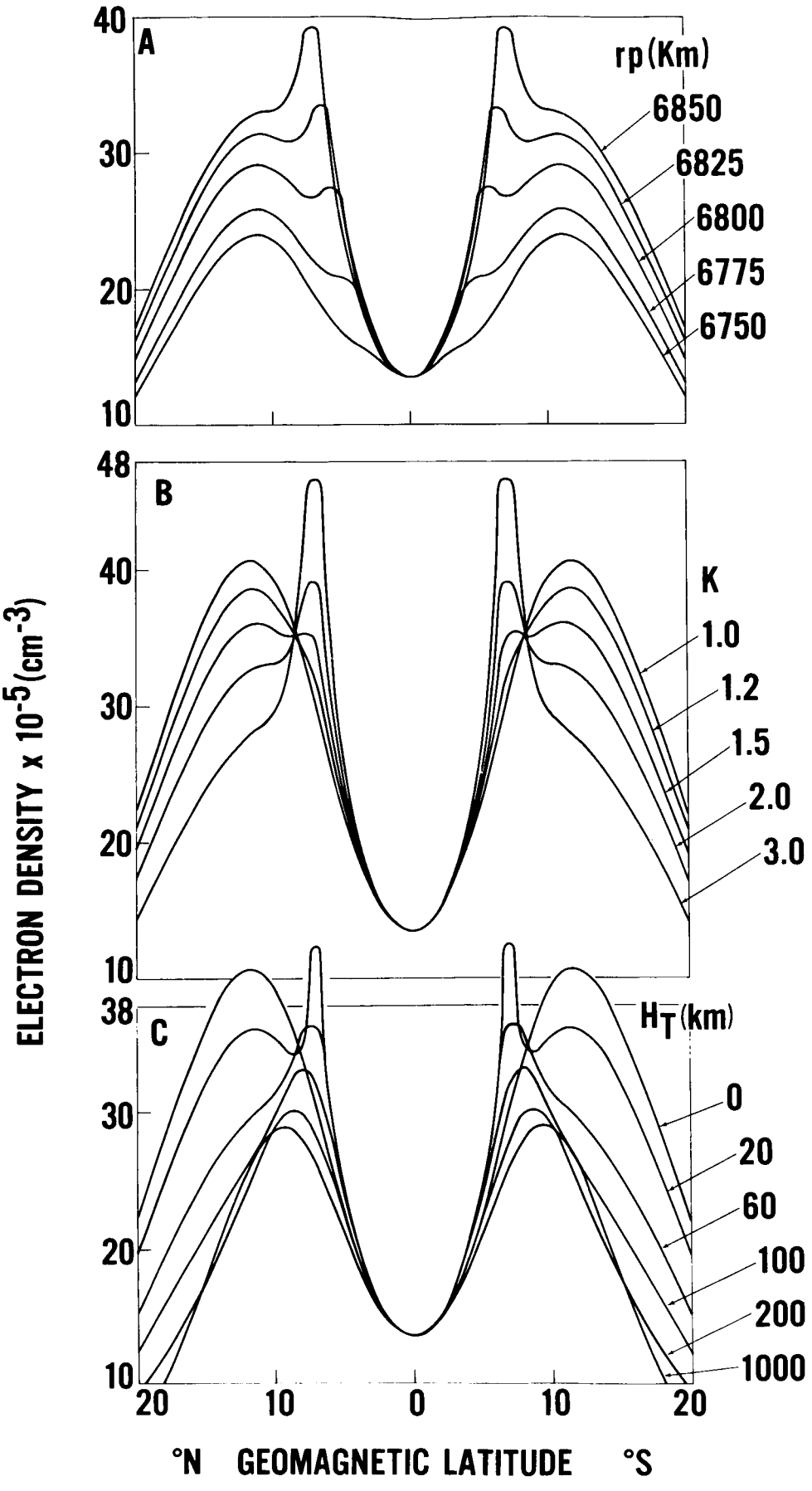
A
rp(Km)
6850
6825
6800
6775
6750
B
K
1.0
1.2
1.5
2.0
3.0
C
H_T(km)
0
20
60
100
200
1000
ELECTRON DENSITY x 10^{-5}(cm^{-3})
°N GEOMAGNETIC LATITUDE °S

Figure 6.

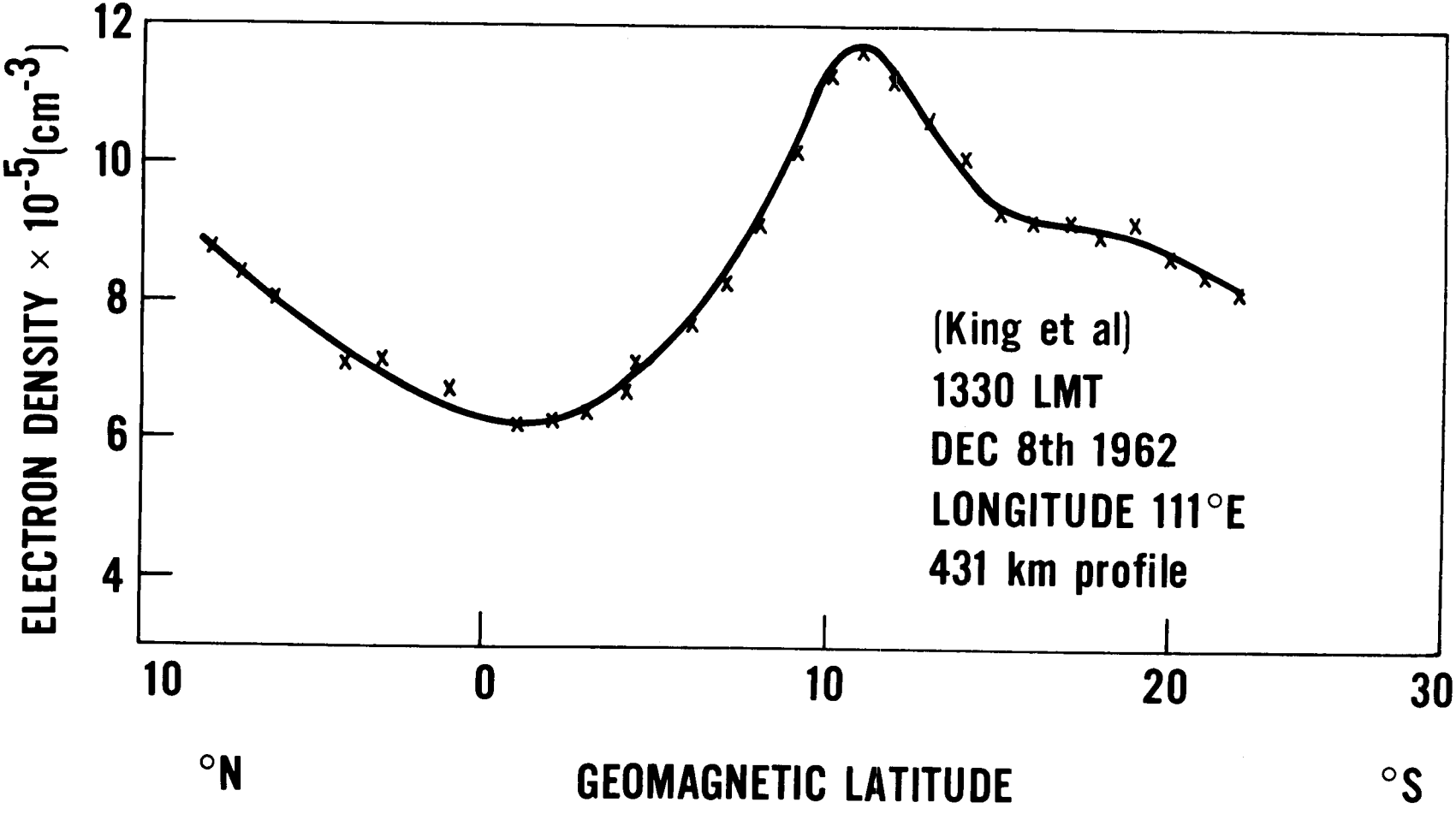
ELECTRON DENSITY × 10-5(cm-3)
12
10
8
6
4
(King et al)
1330 LMT
DEC 8th 1962
LONGITUDE 111°E
431 km profile
10
0
10
20
30
°N
GEOMAGNETIC LATITUDE
°S

Figure 7.

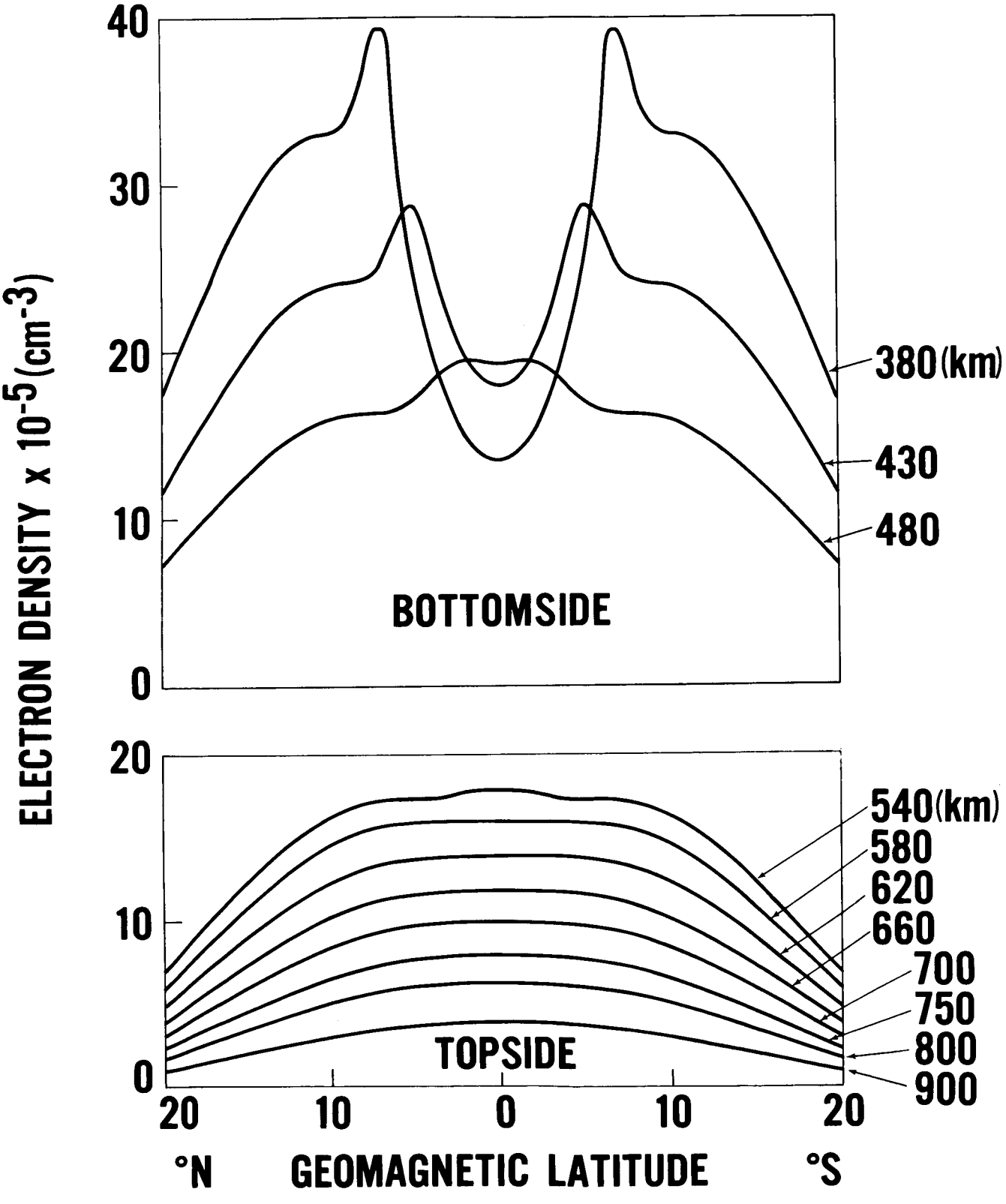
ELECTRON DENSITY x 10^{-5}(cm^{-3})
40
30
20
10
0
380(km)
430
480
BOTTOMSIDE
20
10
0
540(km)
580
620
660
700
750
800
900
TOPSIDE
20
10
0
10
20
°N
GEOMAGNETIC LATITUDE
°S

Figure 8.

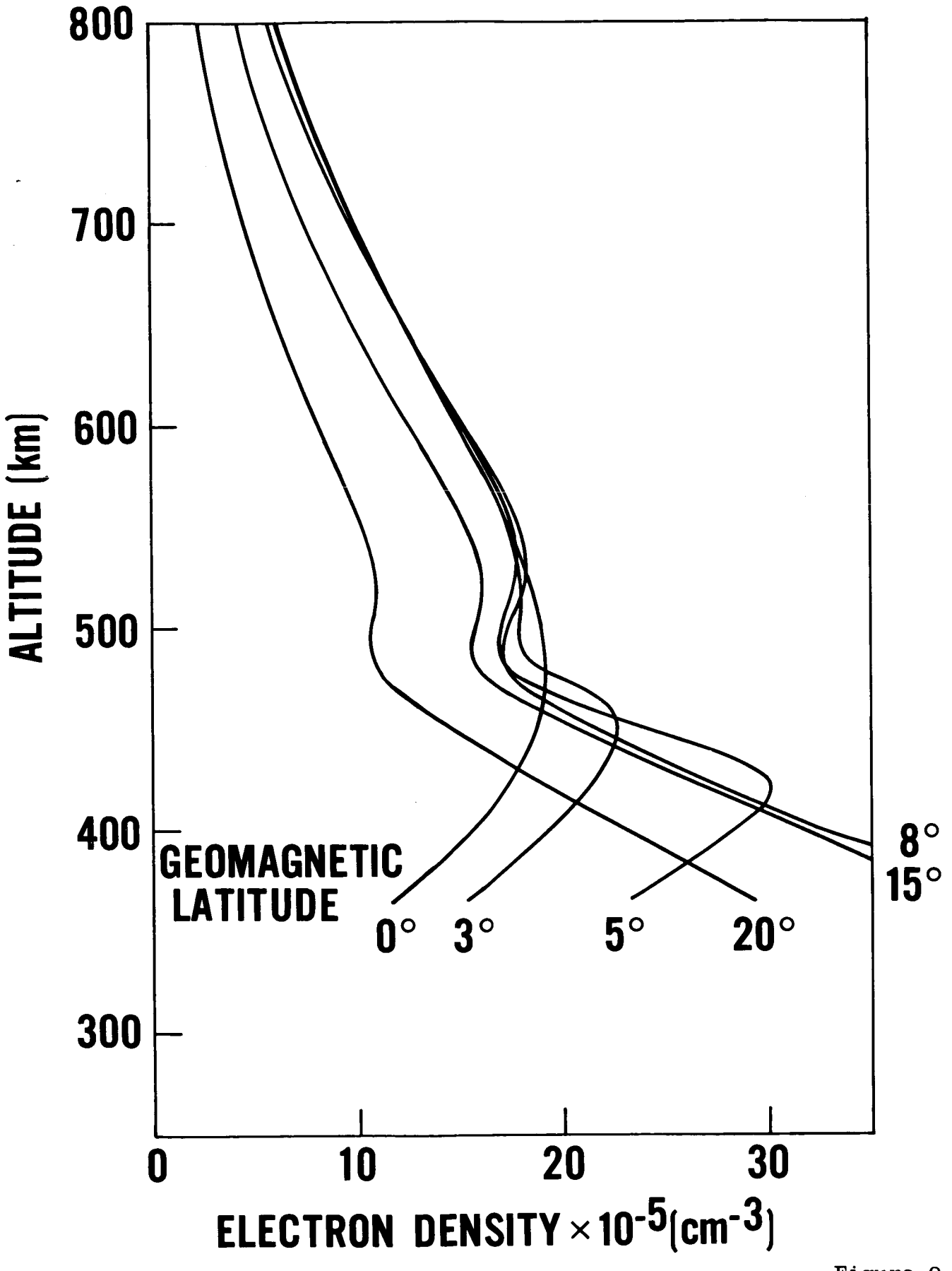
800
700
600
500
400
300
ALTITUDE (km)
GEOMAGNETIC
LATITUDE
0°
3°
5°
20°
8°
15°
0
10
20
30
ELECTRON DENSITY × 10-5(cm-3)

Figure 9.

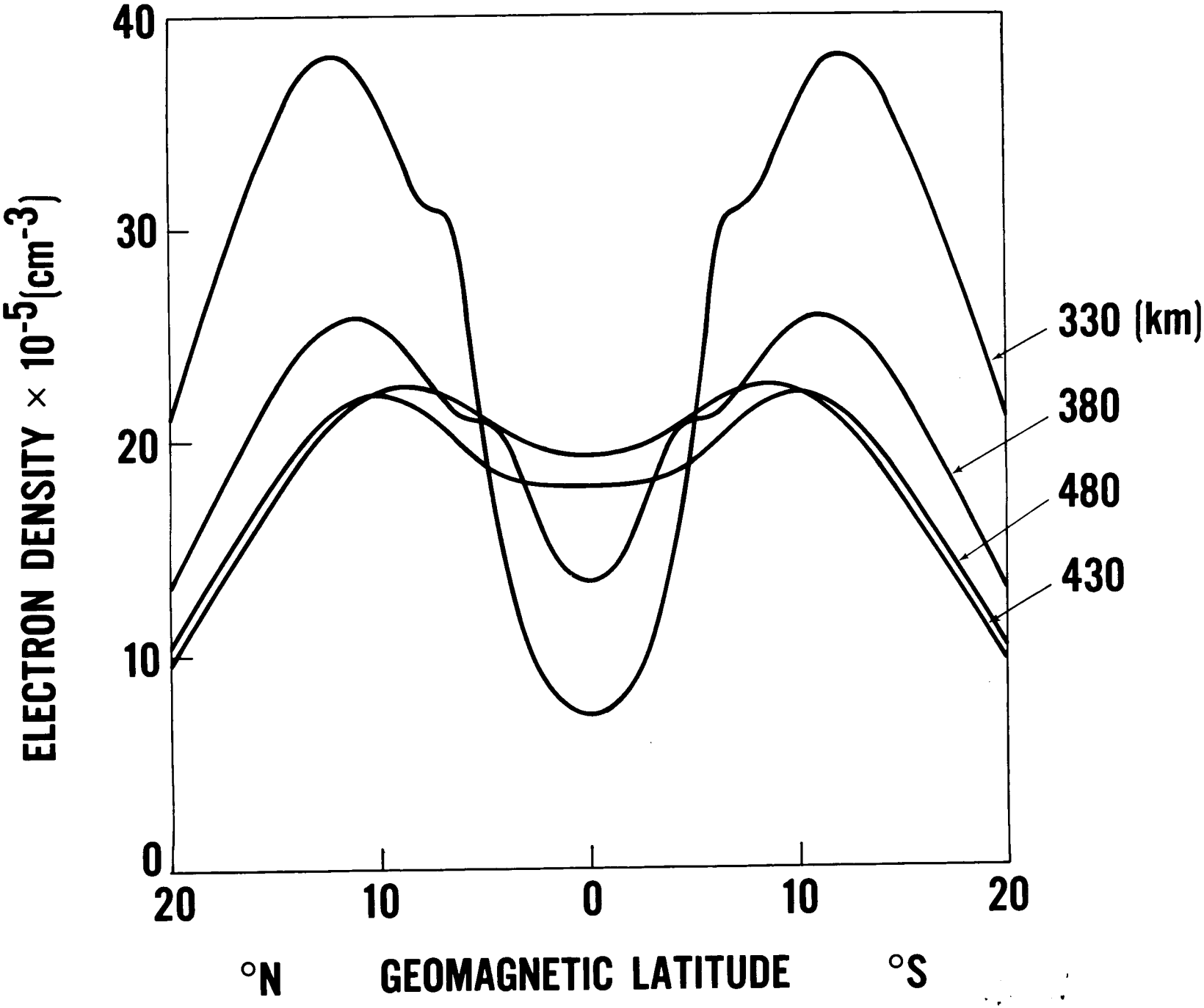
40
30
20
10
0
ELECTRON DENSITY × 10-5(cm-3)
330 (km)
380
480
430
20
10
0
10
20
°N
GEOMAGNETIC LATITUDE
°S

Figure 10.